ACS APPLIED MATERIALS & INTERFACES

Research Article

www.acsami.org

# Self-Assembly and Catalytic Activity of Metal Nanoparticles Immobilized in Polymer Membrane Prepared via Layer-by-Layer Approach

Joydeep Dhar and Satish Patil*

Solid State and Structural Chemistry Unit, Indian Institute of Science, Bangalore 560012, India

Supporting Information

**ABSTRACT:** Densely packed nanoparticles distributed in a stable and robust thin film is a highly preferred system for utilizing the various applications of nanoparticles. Here, we report covalent bond mediated layer-by-layer (LbL) self-assembled thin films of nanoparticles embedded in polymer membrane. Polymer with complementary functional group is utilized for fabrication of thin film via covalent bonding. UV–visible spectroscopy, atomic force microscopy (AFM) and scanning electron microscopy (SEM) were used to monitor the growth of LbL thin film. Subsequently, the composite thin film is used for catalysis of an organic electron transfer reaction of *p*-nitrophenol to *p*-aminophenol by sodium borohydride. The catalytic activity of these composite films is assayed multiple times, proving its applicability as a catalyst. The kinetic data obtained by monitoring reduction of *p*-nitrophenol suggest that the reaction rates are directly related to the sizes of the nanoparticle and porosity of the membrane.

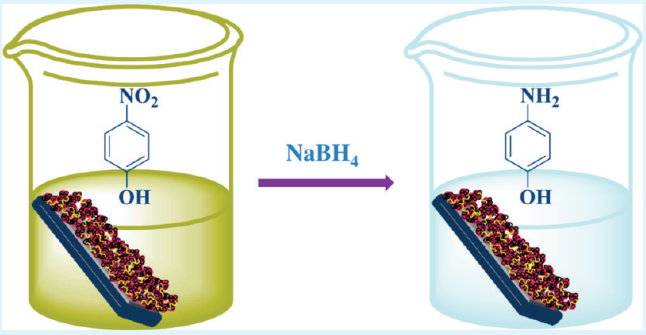


**KEYWORDS:** *nanoparticles, O-carboxymethyl chitosan, nanocomposite, layer-by-layer*

## INTRODUCTION

Nanotechnology illustrates many examples of unique materials with small dimensions, which renders them useful for a wide range of applications. Metal particle in nanometer domain shows distinctive size-dependent optical[1] and electronic properties[2] that are extensively used for different types of applications such as microelectronic devices,[3] electrochemical sensors,[4] nonlinear optics,[5] pharmaceuticals[6] and catalysis.[7] However, a critical challenge is to transfer these nanoparticles on functionalized surfaces while retaining their nanoscale properties. The difficulty is also associated with the sensitivity of these nanoparticles to coalescence and agglomerate on various surfaces because of their high surface to volume ratio. In recent times, much of research efforts have been directed toward the self-assembly of metal nanoparticles onto functionalized surfaces to widen their scope of applications. Normally, small molecules,[8] surfactants,[9] micelles,[10] microgels,[11] latex particles,[12] dendrimers,[13] and polymers[14,15] are used to stabilize nanoparticles. Self-assembled monolayer or multilayered array of nanoparticles in the organic matrix can be introduced by in situ synthesis of metal nanoparticles in presence of polymer or polyelectrolyte,[16] Langmuir–Blodgett techniques[17] and layer-by-layer (LbL) adsorption approach on metal nanoparticles.[18,19]

The LbL technique is a versatile approach to create ultrathin advanced surface coating on a wide range of surfaces. The first layer is adsorbed based on electrostatic interactions and thereafter the deposition is driven by means of electrostatic,[20] H-bonding,[21] covalent,[22] charge transfer[23] or van der Waal's interactions.[24] This technique is well established in forming highly dense and compact ultrathin films from various kinds of organic or polymeric materials, with precise control of layer composition and thickness. The formation of LbL thin film by covalent bonding is a relatively new and emerging area of research.[25,26] The covalent bonded self-assembly offers extra stability to the thin film because the growth is driven by complementary functional group. Using covalent bonded LbL self-assembly, robust and stable thin films can be easily prepared which can withstand harsh conditions. Processing and many related applications demand high mechanical strength and chemical stability of the thin film. Multilayer film formed by covalent bond responds partially with external stimuli as compared to the LbL film grown by other interactions. Bergbreiter et al. created LbL ultrathin film by covalent bonding applying "click" chemistry in azide and alkyne copolymers of poly(*N*-isopropylacrylamide).[27] But there are only few reports where nanoparticles are incorporated in polymer thin film using covalent bond interaction.[28,29] The covalent bond mediated thin film of nanoparticles is mainly restricted to small bifunctional molecules, which can coordinate

Received: January 13, 2012
Accepted: March 8, 2012
Published: March 8, 2012

  

two adjacent nanoparticle layers through their functional groups.[4,30,31] In such an approach, all works relies on the terminal sulfur containing linker molecules which have high affinity toward surface atoms of noble metals.[32] Moreover, entropically it is unfavorable to use small molecules to form ordered structure as entropy loss due to formation of self-assembly is more in comparison with polymer or polyelectrolyte matrix stabilized nanoparticles.[33] Surface modification with polymer also reduces the aggregation of nanoparticles, referred to as steric stabilization.[34]

This paper describes the fabrication of nanocomposite thin film of chitosan and metal nanoparticles via LbL self-assembly. The nanocomposite thin film is achieved by modifying chitosan with carboxymethyl group. The introduction of carboxyl group in the polymeric backbone can serve two purposes. First, it can bind with metal atom and the carboxyl groups on the surfaces can stabilize the nanoparticles by electrostatically repelling the neighboring particles. Moreover, presence of carboxymethyl group renders the solubility of chitosan in water at neutral pH. Finally, the catalytic activity of nanocomposite thin film in the reduction reaction of *p*-nitrophenol to *p*-aminophenol using sodium borohydride was verified and its kinetics fully analyzed.

## EXPERIMENTAL SECTION

**Materials.** Chitosan ($M_W$ 70 000; degree of deacetylation 85%) was purchased from Sigma-Aldrich. Isopropyl alcohol ($C_3H_7OH$) and *p*-nitrophenol (4-$C_6H_5NO_3$) were supplied by SRL Pvt. Limited. Chloroauric acid ($HAuCl_4{\cdot}3H_2O$) was obtained from Kem Light Laboratories Private Limited. Sodium hydroxide (NaOH), hydrochloric acid (HCl), monochloroacetic acid ($ClCH_2COOH$) and hydrazine monohydrate ($N_2H_4{\cdot}H_2O$) were purchased from SD fine chemicals. Silver nitrate ($AgNO_3$) and sodium borohydride ($NaBH_4$) were supplied by Spectrochem. All the experiments were performed in Millipore water having specific resistance 18 MΩ.

**Synthesis of *O*-Carboxymethyl Chitosan (OCC).** Synthesis of OCC from chitosan was performed following reported procedure[35] with some modification. Briefly 0.5 g chitosan was dispersed in 10 mL of isopropyl alcohol for 1 h. Then 2 mL of 5N NaOH solution in Millipore water was added dropwise into chitosan dispersion and stirred for 2 h at room temperature (30 °C) followed by slow addition of 2 g of monochloroacetic acid dissolved in 10 mL isopropyl alcohol. The mixture was allowed to stir for another 4 h. The reaction was quenched by addition of 10 mL of 90% ethyl alcohol. It was filtered off and washed thoroughly with 80% ethyl alcohol. Sodium salt of OCC was suspended in 80% ethyl alcohol and treated with conc. HCl to convert the sodium salt into protonated form of OCC. After filtration it was washed and vacuum-dried.

**Preparation of Polymer Nanocomposite.** Nanocomposite was prepared by in situ reduction of metal salt mixed with polymer solution. OCC (20 mg) was dissolved in 20 mL of Millipore water followed by addition of 5 mg of $HAuCl_4.3H_2O$ with proper stirring for 2 h. Then 0.5 g (2 M) of hydrazine monohydrate dissolved in 5 mL Millipore water was added. Immediately color changed from light yellow to wine red. NaOH was used to make the pH neutral to slightly basic. It was stirred for 2 h. Later, it was centrifuged at 6000 rpm to settle down the nanocomposite and properly washed with water to remove excess hydrazine. It was then vacuum-dried and used for characterization and thin film preparation.

Silver nanocomposite was prepared following the same protocol. $AgNO_3$ was used as precursor salt for synthesizing silver nanoparticles. Other parameters were kept constant during synthesis. We refer to these nanomaterials as polymer nanocomposites throughout the manuscript.

Since it has been reported[36] that gold nanoparticles with diameter smaller than 5 nm exhibit unusual catalytic activity, we have also prepared gold nanocomposite having size around 5 nm in presence of OCC. To synthesize gold nanoparticle with particle size ∼5 nm, 25 mg of OCC was dissolved in 25 mL of water followed by addition of 2.5 mg of $HAuCl_4{\cdot}3H_2O$ and stirred for 2 h. Then 1 mL freshly prepared ice-cold 0.1 N $NaBH_4$ was added dropwise and stirred vigorously for another 2 h to form a nice dispersion of ultra fine gold nanocomposite.

**Preparation of Thin Film.** Polymer nanocomposite solution (0.05 mg/mL) was prepared after sonicating the dried sample for 30 min in Millipore water. The quartz plate was treated with Piranha solution (7:3 v/v conc. $H_2SO_4/H_2O_2$) followed by washing several times with water. Before dipping in acidified solution of OCC (0.5 mg/mL) it was dried under nitrogen flow. After 24 h, it was taken out, washed with water to remove unadsorbed OCC and then dried with nitrogen gas. Subsequently, the plate was immersed in freshly prepared glutaraldehyde solution (0.1 mL/mL in water) and then in polymer nanocomposite solution in a consecutive manner after every 3 h. By repeating this cycle covalent bonded multilayer thin film was fabricated onto a quartz plate and growth was monitored by UV−visible spectroscopy and scanning electron microscopy (SEM). Film morphology was studied by atomic force microscopy (AFM). Following a similar procedure, thin film was prepared on glass substrate, which was later used for application of gold nanocomposite to catalyze an electron transfer reaction.

**Catalytic Activity.** Catalytic activity has been studied by using two glass plates of 40 mm × 25 mm × 1 mm deposited with gold nanocomposite thin film on both the sides. After addition of 0.37 g of sodium borohydride in 100 mL of $3.6 \times 10^{-6}$ (M) *p*-nitrophenol, it is converted into *p*-nitrophenolate. As a result, color of the reaction mixture turned yellowish green from light yellow. Catalytic reaction immediately started after introducing two glass plates with gold nanocomposite thin film in the solution in such a way that these glass plates do not touch each other. Separately, we performed the same reaction with another three pairs of glass plates having 10, 20, and 40 multilayer thin film. Catalytic reaction with 10 and 40 multilayered thin film having smaller sized (5 nm) gold nanoparticles were also performed in similar manner. The reaction was monitored by UV−visible spectroscopy at 400 nm. At regular intervals aliquots were taken out from the solution and UV−visible spectra were recorded at room temperature.

## CHARACTERIZATION

**Spectroscopy.** *UV−Visible Spectroscopy.* Growth of thin film and kinetics of catalysis reaction were monitored using Perkin-Elmer (Lambda 35) Spectrometer. All the experiments were done at room temperature.

*Nuclear Magnetic Resonance (NMR) Spectroscopy.* $^1$H NMR spectra were recorded in Bruker Avance NMR spectrometer at 400 MHz frequency. $D_2O$ and TMS were used as solvent and internal standard, respectively.

*Fourier Transform Infrared (FTIR) Spectroscopy.* Samples were well ground and made into pellets with KBr powder. Spectra were recorded in Perkin-Elmer FT-IR spectrophotometer, spectrum 1000. Attenuated Total Reflectance (ATR) mode FT-IR spectrum was recorded for the 20 multilayered thin film with gold nanocomposite material in Thermo-Nicolet 6700 spectrophotometer using ZnSe crystal.

*Inductively Coupled Plasma-Optical Emission Spectrometry (ICP-OES).* The amount of gold and silver in the composite materials as well as in the thin films used for the catalysis were determined by ICP optical emission spectroscopy using Thermo Scientific-iCAP 6500 ICP spectrometer at $\lambda$ = 242.7 and 328 nm for gold and silver respectively. The samples were prepared by dissolving the thin films and gold nanocomposites in aqua-regia and silver nanocomposite in conc. nitric acid and thereafter diluted with Millipore water. For each sample, three measurements were carried out and the average of those readings are reported.

**Scheme 1. Synthesis of OCC**

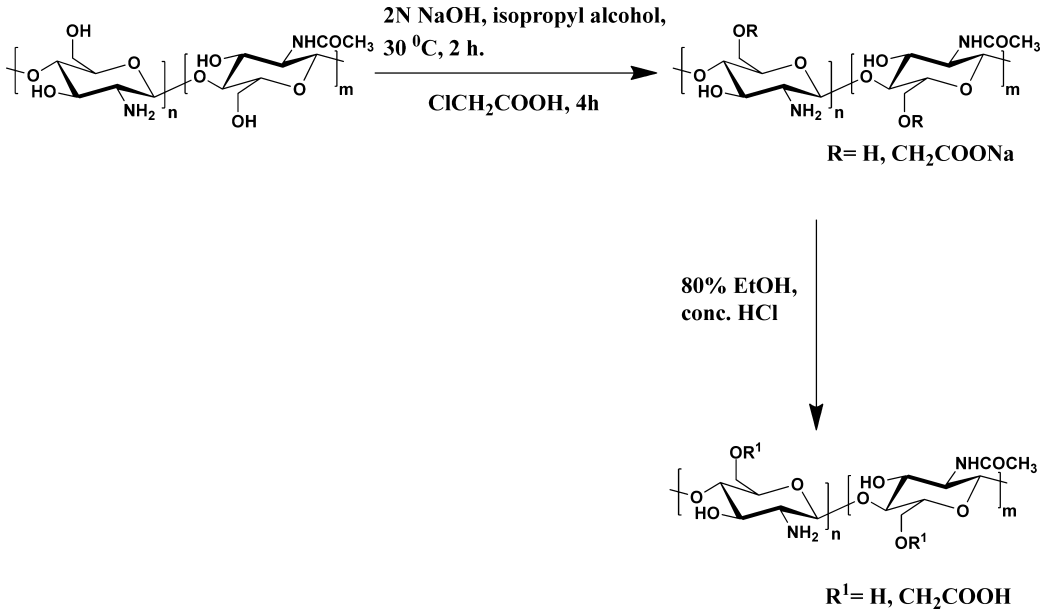


**Microscopy.** *Field-Emission Scanning Electron Microscopy (FESEM).* Samples were prepared by drop-casting the nanocomposite solution on silicon wafer. Thin film samples are fabricated on glass substrate by LbL procedure. Using Sirion and Zeiss scanning electron microscope at different working voltages imaging was performed after platinum coating.

*Transmission Electron Microscopy (TEM).* TEM images were taken in Tecnai T20 field emission microscope at 200 kV in room temperature. A dilute solution of nanocomposite dispersion in water was drop-casted on carbon-coated copper grid and dried in air.

*Atomic Force Microscopy (AFM).* AFM images were obtained by using a Digital, Nanoscape IVA AFM, Veeco Instrument, USA in tapping mode. The thin films were prepared from polymer nanocomposite and glutaraldehyde solutions on glass coverslips after treating with piranha solution. Film morphology was studied after forming 11 layers.

*Powder X-ray Diffraction.* The composition and structural properties of metal nanocomposites were investigated by Philips X-pert diffractometer with Cu K$\alpha$ ($\lambda$ = 1.5418 Å) radiation.

## RESULT AND DISCUSSION

**Synthesis and Characterization of *O*-Carboxymethyl Chitosan (OCC).** OCC was synthesized from chitosan by controlled carboxylation at primary alcoholic group as depicted in Scheme 1. By controlling the reaction parameters such as concentration of NaOH, monochloroacetic acid, temperature, ratio of isopropyl alcohol to water and reaction time, the selective chemical functionlization was achieved at C6 position. The reactivity of primary alcohol group is much higher as compared to other groups on chitosan. By optimizing the reaction conditions the selective deprotonation of primary alcoholic group is achieved which further acts as a good nucleophile to replace chlorine atom from monochloroacetic acid to form OCC exclusively. The FTIR spectra of OCC and chitosan are shown in Figure 1. A new peak appeared at 1741 cm$^{-1}$ in OCC, which is indicative of incorporation of carboxyl group. The peak at 1595 cm$^{-1}$ that corresponds to the amine

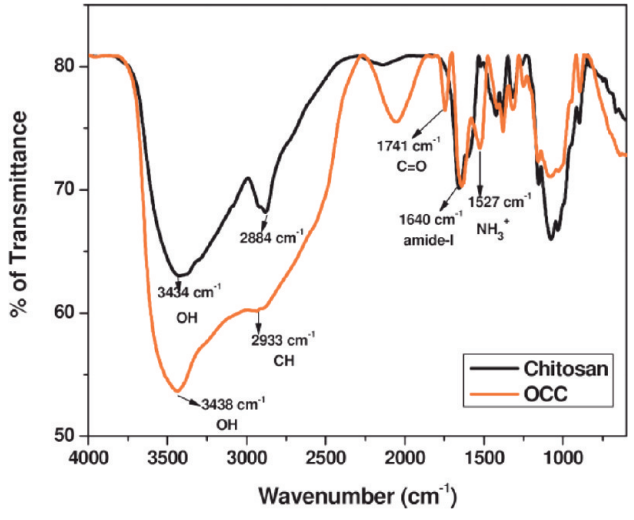


**Figure 1.** FT-IR spectra of OCC.

group of chitosan is shifted to 1527 cm$^{-1}$ in OCC due to protonation. The peak corresponding to OH stretching band in chitosan at 3431 cm$^{-1}$ widened in OCC because of introduction of OH stretching of COOH group and possibly due to extensive H-bonding. The broad peak around 2060 cm$^{-1}$ represents the combination band due to far-IR and $\gamma_2$ frequency of weakly bonded water molecules present in the polymeric network.[37] The FTIR analysis clearly confirms the successful conjugation of carboxyl group to the amine group.

Synthesis of OCC is also confirmed by $^1$H NMR (SI 1). A small new peak which was absent in chitosan appeared at 4.4 ppm in OCC that could be attributed to two carboxymethyl protons in OCC. Absence of any peak at 4.2 ppm confirms that there was no *N*-carboxymethylation. The distinct difference of NMR spectra further confirms the synthesis of OCC and the degree of substitution was calculated from $^1$H NMR as 11%.

OCC retained all the amine functional groups present in chitosan along with the introduction of carboxyl group. Amine group is very important for the self-assembly because it is used


dx.doi.org/10.1021/am300068e | ACS Appl. Mater. Interfaces 2012, 4, 1803−1812

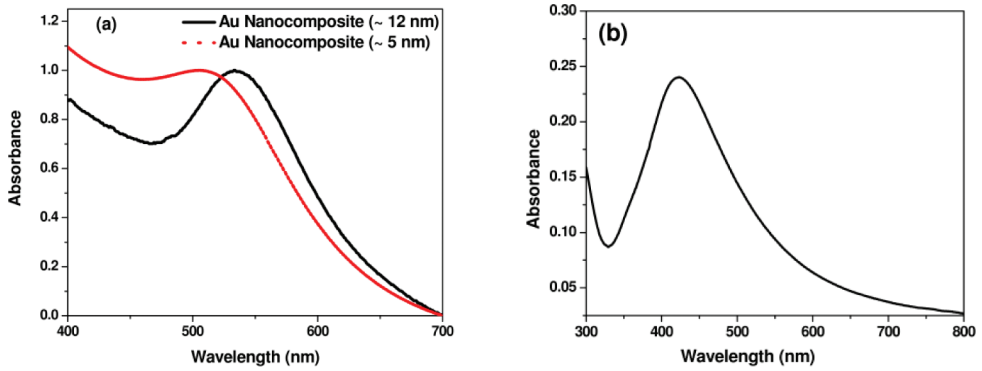


**Figure 2.** UV–visible spectra of (a) gold and (b) silver polymer nanocomposites.

for fabrication of covalent bond mediated thin film as well as stabilization of nanoparticles. Since nitrogen is softer than oxygen, the probability of nitrogen to bind with noble metal surface is more than oxygen due to soft acid soft base interaction, which is energetically more favorable.[32] OCC is completely water-soluble up to pH 12.5.

**Characterization of Polymer Nanocomposites.** OCC is a good chelating agent because it has different ligating group with flexible conformation. Maximum adsorption of $Au^{3+}$ ion by *N*-carboxymethyl chitosan was reported at pH 6.[38] We prepared polymer nanocomposites by dissolving the precursor salt in Millipore water at neutral pH followed by in situ reduction with hydrazine. Surface plasmon resonance (SPR) confirmed the formation of gold and silver nanoparticles. UV–visible spectra of gold and silver nanocomposites are shown in panels a and b in Figure 2, respectively.

Maximum absorption for gold nanoparticle was observed at 533 nm, whereas for silver it was at 423 nm. The absorption maxima for 5 nm gold nanoparticle was blue-shifted to 505 nm as SPR is very much sensitive to size and shape of nanoparticle, dielectric constant of the medium and interparticle distance. For gold nanoparticle below 5 nm with decrease in particle size absorbance peak position tends to shift toward lower wavelength due to quantum size effect.[39] Silver and gold nanocomposite solutions synthesized using hydrazine were greenish yellow and wine red, respectively, in color, whereas it was brownish red for 5 nm gold nanocomposite dispersion. UV–visible absorbance spectrum of silver nanocomposite solution was red-shifted after few days but gold nanocomposite was stable even after 20 days.

Polymer nanocomposites were also characterized by FT-IR spectroscopy (Figure 3). The characteristic peak (1753 $cm^{-1}$) of acid carbonyl group was present in case of gold nanocomposite as it was in OCC but that was not observed for silver. Similarly stretching frequency of OH bond in gold nanocomposite appeared at lower wavenumber as compared to silver nanocomposite which indicates the presence of extensive H-bonding in gold nanocomposite. In case of silver nanocomposite, one broad band centered at 1636 $cm^{-1}$ was observed, due to amide I, NH bending, and stretching vibration of $COO^-$ group. Presence of a band at 1582 $cm^{-1}$ implies the existence of free $NH_2$ group in gold nanocomposite. When we compare the spectra of the composite materials with OCC (SI 2) it can be clearly seen that the OH stretching frequency of COOH is completely disappeared in case of silver nanocomposite and one broad vibration band due to NH and OH stretching of free hydroxyl groups was present around 3430 $cm^{-1}$. This finding can be corroborated by the fact that C═O

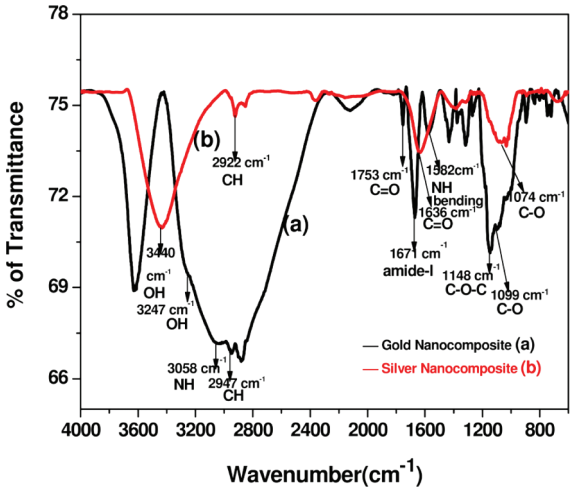


**Figure 3.** FT-IR spectra of (a) gold and (b) silver nanocomposites.

stretching in silver nanocomposite appeared in lower frequency in comparison to OCC and gold nanocomposite due to ionization of carboxyl group. So from the FT-IR spectra it can be concluded that in case of gold nanocomposite $NH_2$ is the main group responsible for stabilizing the nanoparticles whereas COOH group remains on the outer surface of polymer and forms H-bond.[40]

But for silver nanoparticle mostly $COO^-$ as well as $NH_2$ group acts as ligand because silver is a harder Lewis acid than gold.[41]

The amount of metal nanoparticles present in each of the polymer nanocomposite was quantified by ICP-OES analysis and has been given in Table 1. The loading of metal

**Table 1. Estimated Amount of Metal Nanopartcle in Different Nanocomposite Materials**

| polymer composite | metal nanoparticle (mg/10 mg composite) |
|---|---|
| Ag composite | 3.4129 |
| Au composite | 2.152 |
| Au composite (5 nm Au) | 1.2185 |

nanoparticles, i.e., Ag and Au of bigger particle size was higher as compared to that of smaller sized gold nanoparticle. This may be due to the increase in polymer to salt precursor ratio during synthesis of 5 nm gold nanoparticles.

**Electron Microscopy Studies.** Figure 4a shows the SEM image of gold nanocomposite prepared by the drop-cast method, and it has been found the particle size is below 50 nm.

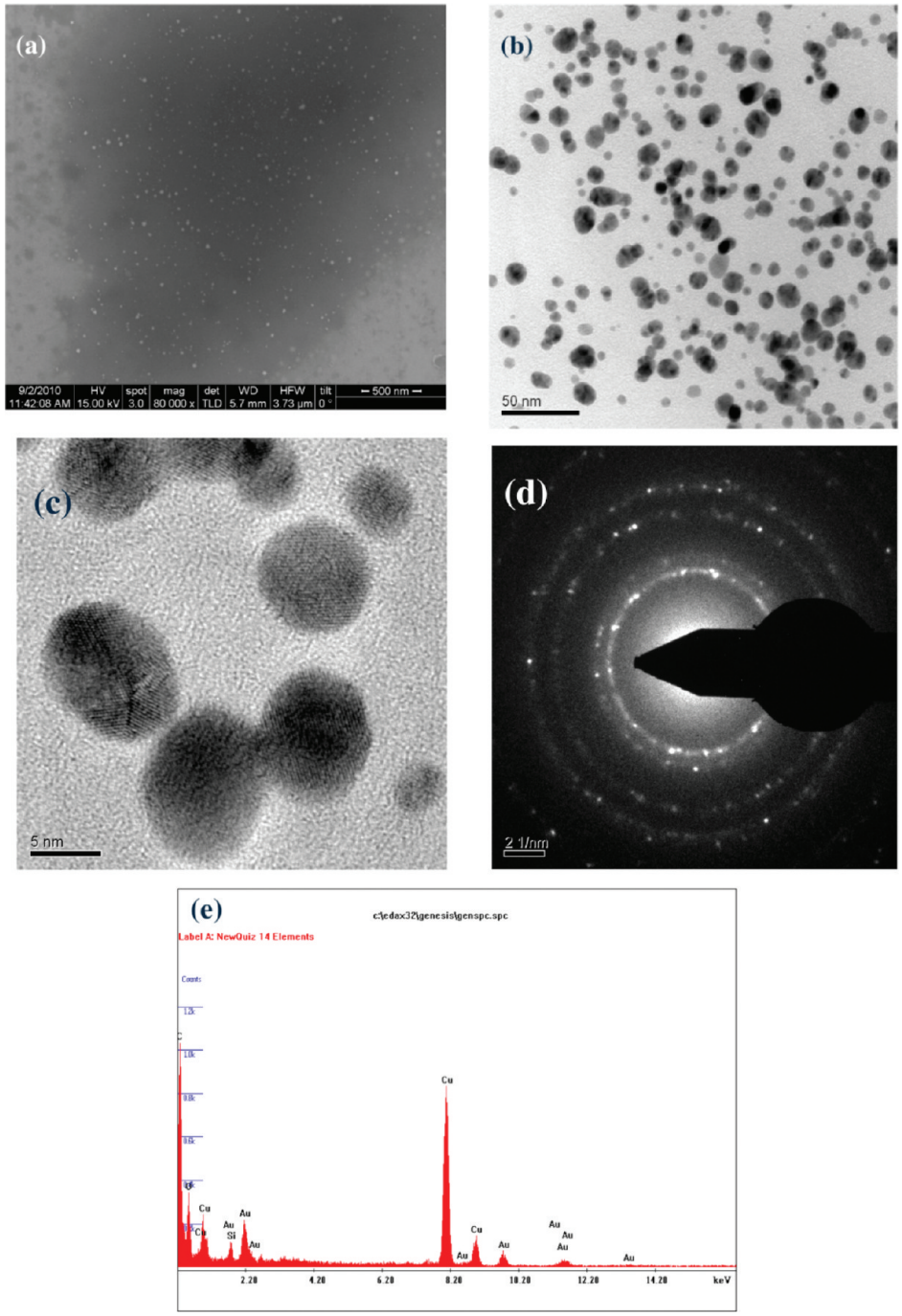


**Figure 4.** (a) SEM, (b) TEM (c), HRTEM images, (d) SAED pattern, and (e) EDS spectrum of gold nanocomposite.

The size and shape of the nanocomposite was confirmed from transmission electron microscopy (Figure 4b, c). Though the particles were not uniform in size, most of the particles had size in between 10 and 20 nm and were almost spherical in shape. Lattice fringes visible in HRTEM image can be correlated with selected area electron diffraction (SAED) pattern of (111), (200), (220), and (311) planes of fcc gold metal and this indicates the polycrystalline nature of the nanocomposite. The elemental analysis in energy dispersive X-ray scattering (EDS) (Figure 4e) confirmed the purity of the nanocomposite. Except the peak due to Au, other peaks of C and O indicate the surface twining of the nanoparticles by the polymer. TEM image of 5 nm gold nanocomposite has been shown in SI 3 in the Supporting Information. From the image, it can be seen that particles are spherical in shape and their diameters are approximately around 5 nm. For silver nanocomposite TEM, HRTEM images, EDS spectra, and SAED pattern are given in Supporting Information (SI 7 and 8).

**Powder XRD Studies.** Polycrystalline nature of polymer nanocomposite is also confirmed by XRD studies. Panels a and b in Figure 5 are the XRD pattern of OCC and polymer nanocomposite, respectively. OCC is amorphous in nature; a broad peak centered at $2\theta = 22°$ is characteristic of chitosan. After nanocomposite formation peaks due to OCC as well as metal nanoparticles both were retained in the diffraction pattern. In gold nanocomposite sharp peaks at $2\theta = 38.35$,


dx.doi.org/10.1021/am300068e | ACS Appl. Mater. Interfaces 2012, 4, 1803−1812

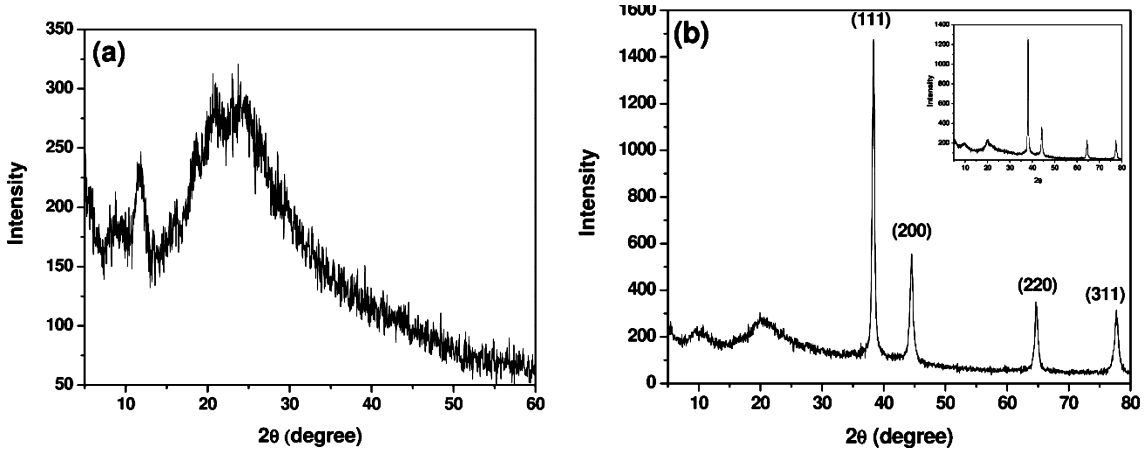


**Figure 5.** Powder XRD pattern of (a) OCC and (b) polymer nanocomposite. Inset shows XRD pattern of silver nanocomposite.

44.55, 64.68, and 77.68° can be assigned as reflection from (111), (200), (220), (311) planes of the gold nanoparticle for cubic (fcc) structure. Similar XRD pattern was observed for silver nanocomposite.

**Growth of Thin Film.** We monitored the growth of thin film by using UV−visible spectroscopy and SEM. Thin film was deposited on flat quartz substrate by LbL technique using covalent bonding approach. First layer was adsorbed by dipping the quartz plate into acidified OCC solution using electrostatic interaction. The next layer was deposited by covalent bond mediated Schiff base formation in glutaraldehyde. Thereafter, consecutive layers were formed by alternately dipping into OCC and glutaraldehyde solution. The UV−visible spectrum of LbL growth of gold nanocomposite thin film is shown in Figure 6. A broad peak that was red-shifted as compared to the

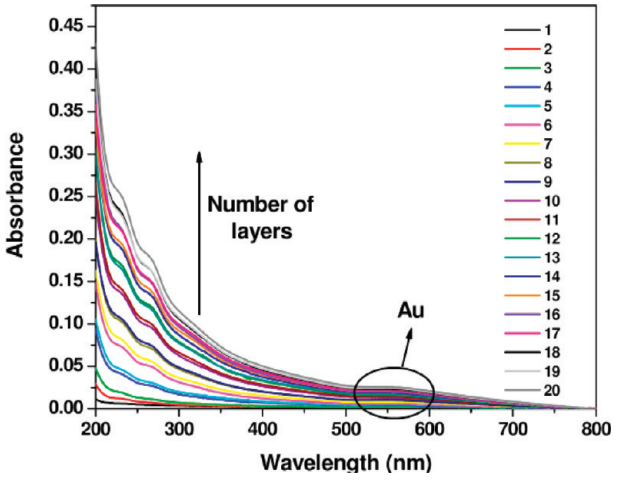


**Figure 6.** LbL growth of gold nanocomposite thin film monitored by UV−visible spectroscopy where odd and even number of layers corresponds to gold nanocomposite and glutaraldehyde adsorption.

solution phase is observed around 540 nm because of SPR of gold nanoparticles. This may be due to increase in refractive index and interparticle coupling, as the distance between two nanoparticles decreases on formation of thin film on solid substrate.

Figure 7 shows the absorbance spectra of those layers in which gold nanoparticles were incorporated into the thin film. Linear growth was observed for each layer adsorption of gold

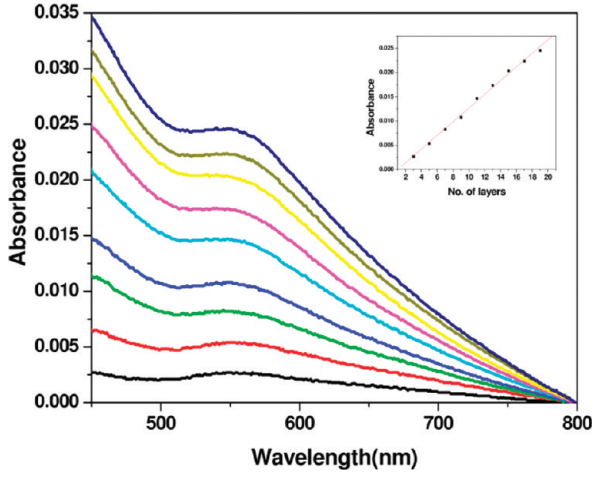


**Figure 7.** UV−visible absorption spectra of gold nanoparticle containing layers. Inset shows the plot of absorbance against number of layers having gold nanoparticles.

nanoparticles as monitored by peak intensity at 545 nm in UV−visible spectra (inset of Figure 7) for 10 bilayers. Signature of glutaraldehyde (at 232 nm), which also showed linear increase after each adsorption step (see SI 4b in the Supporting Information) as glutaraldehyde solution, shows maximum absorption at 233 nm (see SI 4a in the Supporting Information), and confirms the formation of covalent bond mediated self-assembly. Similarly thin film made up of silver nanocomposite using glutaraldehyde also exhibited a broad peak around 425 nm (see SI 6 in the Supporting Information), indicative of SPR of silver nanoparticle. Linear relationship was also observed when maximum absorbance was plotted against number of layers of silver nanoparticle (at 425 nm) as well as for glutaraldehyde (not shown) at 232 nm for 10 bilayers. The covalent bonding between glutaraldehyde and OCC is further confirmed by ATR mode FT-IR spectrum of 20 multilayered gold nanocomposite thin films. The spectrum is provided in the Supporting Information (SI 5).

**Morphology of Thin Film.** Morphology of nanocomposite thin film formed by covalent bonding was also studied by using AFM. The surface of the film containing Au nanoparticles was very rough with $R_{rms}$ value 26.54 nm. The AFM image shown in Figure 8 is collected after depositing 11 layers where the outer surface comprises nanoparticles. These particles were embed-

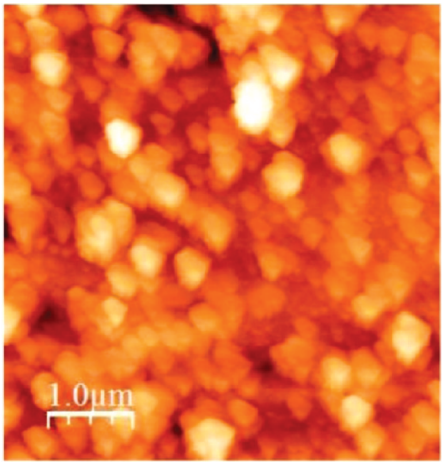


**Figure 8.** AFM height image of 11 layers gold nanocomposite thin film.

ded in the polymeric matrix; as a result, there was no regular shape with specific size distribution and were scattered throughout the film surface with some agglomeration. Single particle diameter observed in AFM is somewhat bigger than what was observed in TEM measurement.

The SEM experiment on 20 layers of nanocomposite thin film also confirms the rough surface texture (Figure 9a). It supports the morphology what was observed in AFM; particles lack proper shape and are distributed densely on the surface. The cross-sectional view of the thin film after depositing 11 layers (Figure 9b) shows uneven surface morphology and the thickness was measured as 42 nm. Film morphology of silver nanocomposite using glutaraldehyde as cross-linker is shown in Supporting Information (SI9). It has been found in both SEM and AFM that particles after being embedded in the polymer matrix lost their shape and were agglomerated. These images provide clear indication that although the particles remain well-dispersed in solution phase, they tend to aggregate on a solid support.

**Catalytic Activity of Gold Nanocomposite Thin Film.** Catalytic activity of gold nanoparticle was demonstrated by the reduction of *p*-nitrophenol to *p*-aminophenol by sodium borohydride. *p*-nitrophenol shows its characteristic absorption maximum at 317 nm; but a red-shift was observed at 400 nm immediately after addition of sodium borohydride. This was due to formation of *p*-nitrophenolate ion. Absorbance remained unchanged until gold nanocomposite thin film was introduced into the solution. Two glass plates deposited with thin film of gold nanocomposite were used to catalyze the reaction. By monitoring the change in absorbance value at 400 nm with time, the progress of the reaction was followed. Size and shape of nanoparticles, polymeric matrix, deposition technique, and total surface area greatly influence the rate of reaction.[42−44] Moreover, interaction between the support and nanoparticle has crucial role in controlling the catalytic activity.[36,40]

Absorbance at time $t = 0$ $(A_0)$ and $t$ $(A_t)$ are proportional to the initial concentration $C_0$ and concentration at time $t$, i.e., $C_t$, of *p*-nitrophenol, respectively. So ratio of $A_0/A_t$ is a measure of $C_0/C_t$. It has been found that the reduction of *p*-nitrophenol to *p*-aminophenol by sodium borohydride in presence of gold nanoparticles as catalyst follows pseudo-first-order rate equation with respect to *p*-nitrophenol because the concentration of sodium borohydride was too high as compared to *p*-nitrophenol. So concentration of sodium borohydride was considered constant throughout the reaction. The rate equation can be written as

$$-d_c/d_t = k_{app}C_t = kSC_t$$

where $k_{app}$ is the apparent rate constant, which is proportional to the surface area $(S)$ available on nanocomposite thin film responsible for catalytic activity. $C_t$ and $k$ are the concentration of *p*- nitrophenol present at time $t$ and normalized rate constant with respect to S respectively. UV−visible spectra of catalytic reduction of *p*-nitrophenol with sodium borohydride in presence of two glass plates having 40 layers of self-assembled thin film is shown in Figure 10. Because the amount of incorporated gold nanoparticles was too low in our thin film the rate of catalytic reaction was very slow. So we did not monitor the reaction until it was complete.

The amount of gold nanoparticles incorporated in the thin films was determined by ICP-OES analysis as given in Table 2. With increase in number of layers the amount of gold nanoparticles present in the thin films increased gradually. But in case of 10 and 40 multilayered thin films with 5 nm nanoparticles, gold content is less than that of 10 layers of self-

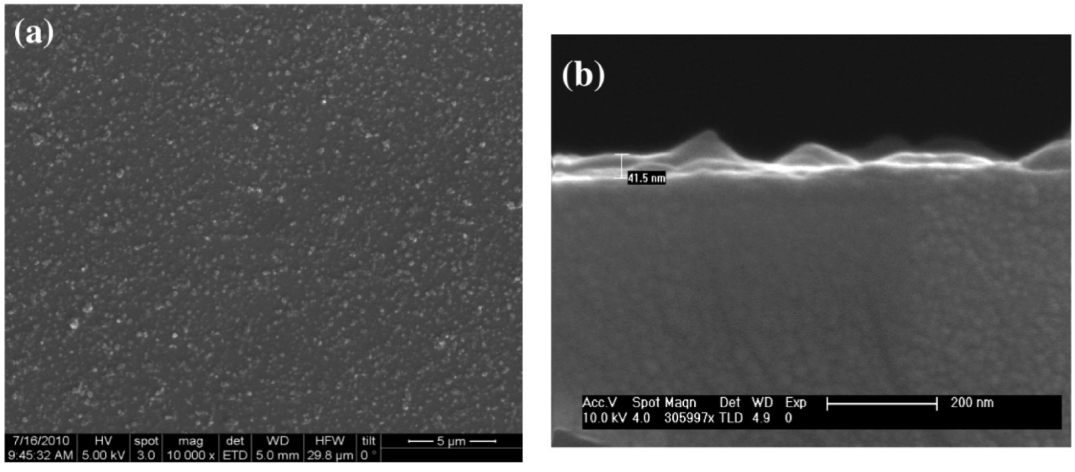


**Figure 9.** (a) Horizontal SEM image of 20 layers gold nanocomposite thin film. (b) Cross-sectional SEM image of 11 layers gold nanocomposite thin film.

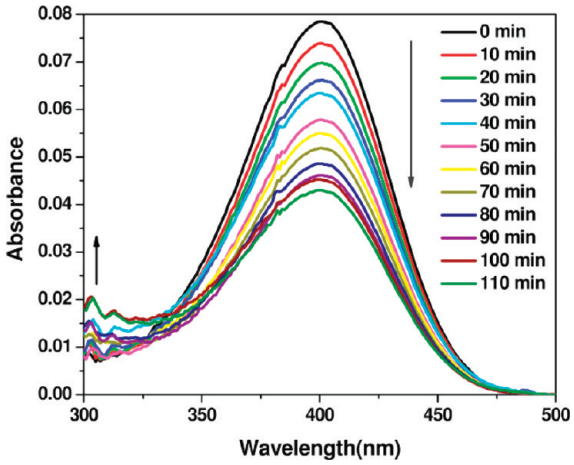


**Figure 10.** UV−visible spectra of reduction of *p*-nitrophenol with sodium borohydride in presence of gold nanocomposite thin film of 40 layers.

**Table 2. Estimated Au by ICP-OES in Different Gold Nanocomposite Thin Films**

| no. of layers | Au (mg) |
|---|---|
| 10 | 0.0045 |
| 20 | 0.0165 |
| 40 | 0.0226 |
| 10 (5 nm) | 0.0012 |
| 40 (5 nm) | 0.004 |

assembled thin film having gold nanoparticles that are bigger in size. The reason behind the less loading of composite material in the thin film in case of smaller sized particles may be the presence of lower amount of gold nanoparticles in the same amount of composite material and increase in polymer content surrounding the nanoparticle's surface providing extra stability against agglomeration as mentioned earlier. The SEM images of the different multilayer thin film before and after the catalytic reaction are given as Supporting Information (SI 10). The density of nanoparticles on the film surface is less for smaller-sized (5 nm) nanoparticles and the particles retained their spherical nature (SI 11). But in case of other nanocomposite thin films particles are densely distributed on the surface and agglomeration was observed.

We have plotted $\ln(C_0/C_t)$ against time for 10, 20, and 40 layers of gold nanocomposite thin films as well as for 5 nm gold nanocomposite films of 10 and 40 layers as catalyst (Figure 11). One significant observation was that the catalytic activity of thin film made of 10 layers (Figure 11a, d) was much higher as compared to 20 and 40 layers (Figure 11b, c, and e) on both cases. This can be explained on the basis of apparent rate constant ($k_{app}$). Calculated $k_{app}$ values of these three films are given in Table 3.

Rate of reaction is directly proportional to the available surface area responsible for catalysis and the amount of catalyst.[45] From Figure 11, it can be seen that 10 layers of self-assembled thin film is far more reactive in comparison to 20 or 40 layers of thin film, though the amount of gold nanoparticles present in 10 layers is comparatively less. This hyper reactivity of 10 layers film may be solely due to availability of higher porosity of the membrane.[46] The kinetics of the reaction is mainly governed by the adsorption of reactants on the surface of catalyst as well as diffusion of *p*-nitrophenol or borohydride

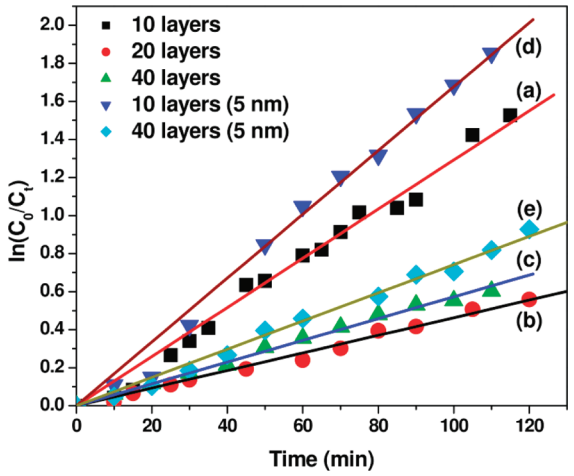


**Figure 11.** Plot of $\ln(C_0/C_t)$ against time for reduction of *p*-nitrophenol to *p*-aminophenol by sodium borohydride in presence of gold nanocomposite multilayer thin film (a) 10, (b) 20, (c) 40, (d) 10 (5 nm) and (e) 40 layers (5 nm).

**Table 3. Apparent Rate Constant Values of Different Gold Nanocomposite Thin Film**

| no. of layers | $k_{app}$ per plate ($min^{-1}$) | $k_{app}$ per plate ($min^{-1}$ $mg^{-1}$) |
|---|---|---|
| 10 | 0.0064 | 1.4222 |
| 20 | 0.0024 | 0.1454 |
| 40 | 0.0028 | 0.1239 |
| 10 (5 nm) | 0.0083 | 7.1367 |
| 40 (5 nm) | 0.0037 | 0.925 |

through the film.[47] The porosity in LbL self-assembly decreases as a function of number of layers; hence it would hinder the diffusion of *p*-nitrophenol molecule through the polymer layers. This assumption could be attributed that, the surface area, needed for the electron transfer to take place has reduced in case of thin films with higher number of layers. But the $k_{app}$ value of 40 layers film (Figure 11c) is slightly higher than that of 20 layers (Figure 11b). This slight variation may be due to higher loading of gold nanoparticles in 40 layers film. We found that the $k_{app}$ value for the 10 layers film dropped down to 0.0055 $min^{-1}$ in the next catalytic cycle, but for the other two films, it remained almost the same (0.0023 and ∼0.0028 $min^{-1}$ for 20 and 40 layers films, respectively). This signifies that although the 10 layers film is more reactive than the other two, the 20 and 40 layer films were found to be more stable. From SEM images, it can be seen that film morphology is changed before and after the two cycles of catalytic reaction for the 10 multilayered thin film (SI 10b in the Supporting Information) but it remained the same for the 40 layers film (SI 10d in the Supporting Information). Because the stability of the 10 layers film was not so high, we cannot rule out the possibility of its higher reactivity being due to the presence of free particle coming out in the reaction medium as a consequence of the leaching out of the film. We have compared the reactivity of the thin films made up of very small gold nanoparticles (5 nm) with that of gold nanocomposite with particles of bigger size. Though the amount of gold nanoparticles (5 nm) incorporated in 10 and 40 multilayered thin films were very low but they showed higher reactivity as compared to their vis-à-vis. Because the amount of nanoparticles loaded for the same number of layers were different for two systems with regard to the particle size, we have calculated the $k_{app}$/mg of gold nanoparticles. It

has been found that the reaction rates were five and six times higher, respectively, with the thin films of 10 and 40 layers of 5 nm gold nanoparticles though the number of particles present on the surface were lower as observed from SEM images. The particles that are distributed on the surface mainly take part in the reaction, as accessibility of those particles embedded in the polymeric thin film decreases because of the compactness of the covalently bonded thin film as a function of number of layers.

## CONCLUSION

In conclusion, we have demonstrated that the covalent bond mediated LbL self-assembly can be utilized to immobilize metal nanoparticles to ensure their stability against aggregation. The porosity present in polymer membrane provides the driving force for diffusion of *p*-nitrophenol by creating concentration gradient from aqueous medium to reaction center to accelerate the reaction rate. Films having lesser number of layers (10 layers) show higher catalytic activity in comparison to the films of higher number of layers (20, 40 layers). But in respect to stability, films with higher number of layers are much better. Moreover, the size of the nanoparticles plays a crucial role in determining the catalytic activity, as observed from our study. So there should be an optimization in preparation of these films to employ them as electron transfer catalyst. Though the catalytic activity of these films is low, by modulating number of layers in the LbL film, highly catalytic active and stable films can be fabricated by this simple and versatile approach.

## ASSOCIATED CONTENT

### Supporting Information

Additional figures (PDF). This material is available free of charge via the Internet at http://pubs.acs.org.

## AUTHOR INFORMATION

### Corresponding Author

*Tel: +91-80- 22932651. Fax: +91-80-23601310. E-mail: satish@sscu.iisc.ernet.in.

### Notes

The authors declare no competing financial interest.

## ACKNOWLEDGMENTS

The authors thank Council of Scientific and Industrial Research and Indian Institute of Science for providing the grant to carry out the research work. The assistance of Centre for Nano Science and Engineering, Nano centre, NMR centre, Spectroscopy and Analytical Facility, IISc., and Veeco-India Nanotechnology Laboratory for SEM, TEM, NMR, ICP-OES, and AFM measurements are gratefully acknowledged.

## REFERENCES

(1) Shon, Y. S.; Dawson, G. B.; Porter, M.; Murray, R. W. *Langmuir* **2002**, *18*, 3880−3885.
(2) Nishida, N.; Shiraishi, Y.; Kobayashi, S.; Toshima, N. *J. Phys. Chem. C* **2008**, *112*, 20284−20290.
(3) Simon, U.; Schon, G.; Schmid, G. *Angew. Chem., Int. Ed.* **1993**, *32*, 250−254.
(4) Abdelrahman, A. I.; Mohammad, A. M.; Okajima, T.; Ohsaka, T. *J. Phys. Chem. B* **2006**, *110*, 2798−2803.
(5) Collier, C. P.; Saykally, R. J.; Shiang, J. J.; Henrichs, S. E.; Heath, J. R. *Science* **1997**, *277*, 1978−1981.
(6) Mani, V.; Chikkaveeraiah, B. V.; Patel, V.; Gutkind, J. S.; Rusling, J. F. *ACS Nano* **2009**, *3*, 585−594.
(7) Pradhan, N.; Pal, A.; Pal, T. *Colloid Surf., A* **2002**, *196*, 247−257.
(8) Turkevic., J; Kim, G. *Science* **1970**, *169*, 873−879.
(9) Yonezawa, T.; Tominaga, T.; Toshima, N. *Langmuir* **1995**, *11*, 4601−4604.
(10) Bae, K. H.; Choi, S. H.; Park, S. Y.; Lee, Y.; Park, T. G. *Langmuir* **2006**, *22*, 6380−6384.
(11) Biffis, A.; Orlandi, N.; Corain, B. *Adv. Mater.* **2003**, *15*, 1551−1555.
(12) Chen, C. W.; Chen, M. Q.; Serizawa, T.; Akashi, M. *Adv. Mater.* **1998**, *10*, 1122−1126.
(13) Esumi, K.; Isono, R.; Yoshimura, T. *Langmuir* **2004**, *20*, 237−243.
(14) Hirai, H.; Nakao, Y.; Toshima, N. *Chem. Lett.* **1978**, 545−548.
(15) Mbhele, Z. H.; Salemane, M. G.; van Sittert, C.; Nedeljkovic, J. M.; Djokovic, V.; Luyt, A. S. *Chem. Mater.* **2003**, *15*, 5019−5024.
(16) Joly, S.; Kane, R.; Radzilowski, L.; Wang, T.; Wu, A.; Cohen, R. E.; Thomas, E. L.; Rubner, M. F. *Langmuir* **2000**, *16*, 1354−1359.
(17) Chen, S. W. *Langmuir* **2001**, *17*, 2878−2884.
(18) Decher, G. *Science* **1997**, *277*, 1232−1237.
(19) Wang, D. Y.; Caruso, F. *Chem. Mater.* **2002**, *14*, 1909−1913.
(20) Donath, E.; Sukhorukov, G. B.; Caruso, F.; Davis, S. A.; Mohwald, H. *Angew. Chem., Int. Ed.* **1998**, *37*, 2202−2205.
(21) Lutkenhaus, J. L.; Hrabak, K. D.; McEnnis, K.; Hammond, P. T. *J. Am. Chem. Soc.* **2005**, *127*, 17228−17234.
(22) Manna, U.; Dhar, J.; Nayak, R.; Patil, S. *Chem. Commun.* **2010**, *46*, 2250−2252.
(23) Shimazaki, Y.; Mitsuishi, M.; Ito, S.; Yamamoto, M. *Langmuir* **1997**, *13*, 1385−1387.
(24) Kida, T.; Mouri, M.; Akashi, M. *Angew. Chem., Int. Ed.* **2006**, *45*, 7534−7536.
(25) Stroock, A. D.; Kane, R. S.; Weck, M.; Metallo, S. J.; Whitesides, G. M. *Langmuir* **2003**, *19*, 2466−2472.
(26) Brust, M.; Etchenique, R.; Calvo, E. J.; Gordillo, G. J. *Chem. Commun.* **1996**, 1949−1950.
(27) Bergbreiter, D. E.; Chance, B. S. *Macromolecules* **2007**, *40*, 5337−5343.
(28) Wang, J. Y.; Chen, W.; Liu, A. H.; Lu, G.; Zhang, G.; Zhang, J. H.; Yang, B. *J. Am. Chem. Soc.* **2002**, *124*, 13358−13359.
(29) Lu, C. H.; Donch, I.; Nolte, M.; Fery, A. *Chem. Mater.* **2006**, *18*, 6204−6210.
(30) Musick, M. D.; Keating, C. D.; Keefe, M. H.; Natan, M. J. *Chem. Mater.* **1997**, *9*, 1499−1501.
(31) Cassagneau, T.; Mallouk, T. E.; Fendler, J. H. *J. Am. Chem. Soc.* **1998**, *120*, 7848−7859.
(32) Nath, S.; Ghosh, S. K.; Kundu, S.; Praharaj, S.; Panigrahi, S.; Pal, T. *J. Nanopart. Res.* **2006**, *8*, 111−116.
(33) Rahme, K.; Oberdisse, J.; Schweins, R.; Gaillard, C.; Marty, J. D.; Mingotaud, C.; Gauffre, F. *ChemPhysChem* **2008**, *9*, 2230−2236.
(34) Heller, W.; Pugh, T. L. *J. Polym. Sci.* **1960**, *47*, 203−217.
(35) Chen, X. G.; Park, H. J. *Carbohydr. Polym.* **2003**, *53*, 355−359.
(36) Haruta, M. *Catal. Today* **1997**, *36*, 153−166.
(37) Max, J. J.; Chapados, C. *J. Phys. Chem. A* **2004**, *108*, 3324−3337.
(38) Ngah, W. S. W.; Liang, K. H. *Ind. Eng. Chem. Res.* **1999**, *38*, 1411−1414.
(39) Balamurugan, B.; Maruyama, T. *Appl. Phys. Lett.* **2005**, *87*, 143105(1−3).
(40) Liu, W.; Yang, X. L.; Xie, L. *J. Colloid Interface Sci.* **2007**, *313*, 494−502.
(41) Pearson, R. G. *J. Am. Chem. Soc.* **1963**, *85*, 3533−3539.
(42) Rashid, M. H.; Mandal, T. K. *Adv. Funct. Mater.* **2008**, *18*, 2261−2271.
(43) Wang, A. L.; Yin, H. B.; Lu, H. H.; Xue, J. J.; Ren, M.; Jiang, T. S. *Langmuir* **2009**, *25*, 12736−12741.
(44) Schrinner, M.; Polzer, F.; Mei, Y.; Lu, Y.; Haupt, B.; Ballauff, M.; Goldel, A.; Drechsler, M.; Preussner, J.; Glatzel, U. *Macromol. Chem. Phys.* **2007**, *208*, 1542−1547.
(45) Panigrahi, S.; Basu, S.; Praharaj, S.; Pande, S.; Jana, S.; Pal, A.; Ghosh, S. K.; Pal, T. *J. Phys. Chem. C* **2007**, *111*, 4596−4605.
(46) Tokarev, I.; Minko, S. *Adv. Mater.* **2010**, *22*, 3446−3462.

(47) Wunder, S.; Polzer, F.; Lu, Y.; Mei, Y.; Ballauff, M. *J. Phys. Chem. C* **2010**, *114*, 8814−8820.